Biophysical Chemistry 157 (2011) 16–23

Contents lists available at ScienceDirect

Biophysical Chemistry

journal homepage: http://www.elsevier.com/locate/biophyschem

Computational investigation of the enzymatic mechanisms of phosphothreonine lyase

Qiang Pei [a,*], Andrew Christofferson [a], Hui Zhang [b], Jijie Chai [c], Niu Huang [a]

[a] Niu Huang Lab, National Institute of Biological Sciences, Beijing, PR China
[b] School of Chemical and Environmental Engineering, Harbin University of Science and Technology, Harbin, Heilongjiang, PR China
[c] Jijie Chai Lab, National Institute of Biological Sciences, Beijing, PR China

ARTICLE INFO

Article history:
Received 22 January 2011
Received in revised form 2 April 2011
Accepted 3 April 2011
Available online 9 April 2011

Keywords:
SpvC
β-elimination
Michael-addition
Phosphothreonine lyase

ABSTRACT

SpvC, a virulence effector injected through type III secretion system by some *Salmonella serovars*, belongs to the newly discovered enzyme family, phosphothreonine lyase. Previous experimental studies have demonstrated that SpvC irreversibly inactivates mitogen-activated protein kinases by removing the phosphate group from phosphothreonine-containing substrate through a β-elimination mechanism, and results in a β-methyldehydroalanine product. Interestingly, further biochemical investigations also indicated a secondary reaction occurring other than elimination, where a covalently bound complex is formed. Here, we employed molecular dynamics simulations and quantum mechanics calculations to gain insights on the microscopic details of such novel reaction mechanisms. Our theoretical results are consistent with the experimental observations, in which the critical stages of SpvC catalyzed reaction are revealed and the roles of several important binding site residues are reconciled. The deprotonation and precise position of the catalytic base K136 are facilitated by the formation of the fully desolvated active site upon substrate binding. The abstraction of the alpha hydrogen by K136 and the elimination of the phosphate group occur nearly simultaneously, promoted by the proton donation from the catalytic acid H106, and thus strongly supports an E2-like mechanism. K104, which is not directly involved in the enzymatic reaction, stabilizes the transition state and facilitates the reaction to occur. Remarkably, the subsequent deprotonation of K136 happens to be a natural sequel of the primary elimination reaction, restores its nucleophile capacity to attack the double bond containing elimination product, and leads to a covalently bound complex via a Michael-addition mechanism. The reaction mechanism used by phosphothreonine lyases might serve as a method of programmed regulation to fine tune their enzymatic activity.

1. Introduction

Mitogen-activated protein kinases (MAPKs) play an important role in activating immune responses, which are evolutionally conserved in both plants and animals [1–4]. Pathogenic bacteria inactivating host MAPK signaling pathway can repress host innate immunity [5,6]. A newly discovered enzyme family – phosphothreonine lyase – belongs to Gram-negative bacterial pathogenic type III Secretion System (TTSS) effectors, including SpvC from nontyphoid *Salmonella* species, HopAI1 from plant pathogen *Pseudomonas syringae* and OspF from *Shigella* spp [6–10]. These enzymes can permanently inactivate the host MAPKs by cleaving the C_β—O_γ bond from phosphothreonine (pT) containing MAPK activation loop and produce the unnatural amino acid β-methyldehydroalanine (Mdha) [9–12]. Such catalytic activity, without involving any cofactors or metal ions, is unique in current known enzymes with respect to their function of carrying out β-elimination of phosphothreonine or phosphoserine (pS) containing peptide substrates. Moreover, phosphothreonine lyases may hold promise as drug targets in fighting against the pathogenic bacteria, and understanding of their catalyzed reactions will facilitate the discovery of novel antibiotics (i.e. transition state analog design).

Crystal structures of SpvC itself and its inactive mutants complexed with substrate peptides clearly reflect the conformational changes upon substrate binding, where strong electrostatic interactions between positively charged binding site residues (i.e. K104, H106, R148, R213 and R220) and phosphate group of pT183, as well as the hydrophobic interactions between residues F86 and V149 and methyl group of pT183 contribute to forming a fully desolvated substrate binding pocket (Fig. 1) [9,11]. Lysine has a pKa near 7 (pKa = 6 to 7 in most cases). The two protonatable groups of the imidaloze ring can function as hydrogen bond donors and acceptors over a wide range of pH, and play roles as both catalytic acid and base [13–15]. In previous

* Corresponding author at: National Institute of Biological Sciences, No. 7 Science Park Road, Zhongguancun Life Science Park, Beijing, 102206, PR China. Tel.: +86 10 80720645; fax: +86 10 80720813.
E-mail address: polazh@gmail.com (Q. Pei).

0301-4622/$ – see front matter © 2011 Elsevier B.V. All rights reserved.
doi:10.1016/j.bpc.2011.04.002

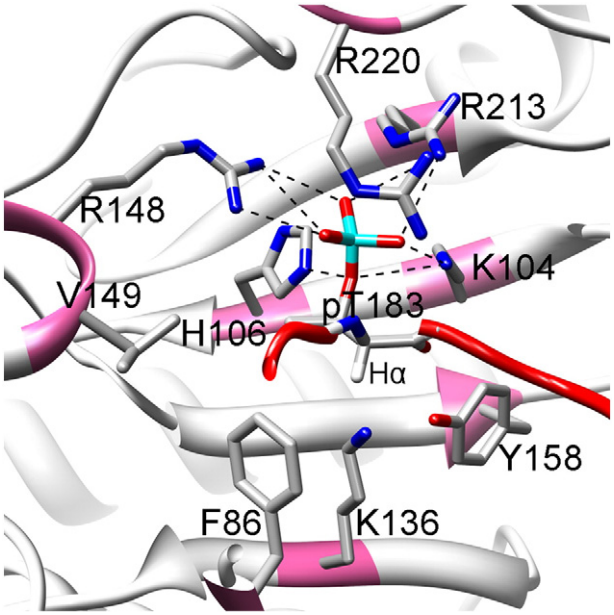

Fig. 1. Specific recognition of phosphothreonine by SpvC. K136 is modeled according to the crystal structure of apo SpvC (PDB: 1Z8M). Protein is represented as gray ribbon and substrate peptide in red ribbon, binding site residues are highlighted as pink ribbon and shown in stick representation. Hydrogen bonds between phosphate moiety of pT183 and binding site residues are represented by dashed lines. C, O, N, H and P atoms are colored in gray, red, blue, white and cyan, respectively. All H atoms except H_α of pT183 are omitted for clarity. Images generated with Chimera [44].

studies of SpvC and its family members, the structural evidence combined with biochemical assays strongly support a β-elimination reaction mechanism, in which the highly conserved residue K136 acts as catalytic base to abstract the H_α from pT183 and H106 acts as a catalytic acid to donate a proton to phosphate group, thus, the C_β—O_γ bond is broken and a C_α C_β double bond is formed [9,11].

However, SpvC was also reported to react with a dehydroalanine (Dha) containing peptide, but insensitive to Mdha, and K136 was proposed to act as a nucleophile to attack the unsaturated C_β atom of Dha and form a covalently bound complex via nucleophilic addition mechanism [9]. Similarly, we detected a covalently bound SpvC–peptide complex in addition to primary β-elimination product (the experimental procedure and results are described in supporting information). The amount of covalently linked complex was progressively increased over time, whereas both SpvC and substrate peptide were decreased, and larger amount of product was produced from a T183S substrate mutant compared to the wild type substrate (Fig. S1). Apparently, SpvC is suicidally inhibited by covalently interacting with the substrate and terminating the enzymatic cycle, which may provide additional information for developing novel antibiotics in inhibiting the pathogenic bacteria. A similar suicide inhibition mechanism has been found in several cases, such as alpha-oxamine synthases [16] and lysine 5,6-aminomutase [17].

Over the last couple of decades, computational chemistry techniques have improved dramatically due to the rapid advances in computer power and extensive efforts in algorithm development [18]. Quantum mechanics (QM) in combination with molecular mechanics (MM) have been increasingly applied in elucidating the mechanism of enzyme catalyzed reactions [19–24]. Here, we employed molecular dynamics (MD) simulations and QM calculations to elucidate the SpvC catalyzed reactions, including the precise reaction mechanisms underlying such novel functions, the critical stages occurring along the reaction pathways and the detailed structural events and energetic consequences contributed by the important binding site residues.

2. Methods

2.1. MD simulations

From experimental estimation, K136 of SpvC plays a crucial role as the key catalytic residue. In order to explore the behavior of K136 during the enzymatic reaction, a total of four reactant complexes were constructed for both SpvC-Erk2 and its T183S mutant with the consideration of K136 in both protonated and deprotonated forms. The wild type enzyme-substrate complex (referred to as SpvC-Erk2 hereafter) was modeled using the crystal structure of inactive SpvC K136A mutant complexed with a phosphothreonine containing Erk2 peptide (PDB ID 2Z8P), in which the coordinates of K136 are assigned according to the SpvC ligand-free structure (PDB ID 2Z8M) [11]. The Erk2 T183S mutant complex (SpvC-T183S) was modeled by replacing the methyl group of pT183 with a hydrogen atom. All treatments are essentially the same in SpvC-Erk2 and SpvC-T183S systems, and thereafter only the SpvC-Erk2 system will be described in this subsection unless otherwise noted. The protonation states of other titratable residues were carefully checked by visual analysis based on their local environment (e.g. the putative catalytic acid H106 was protonated). SpvC-product complexes (referred to as SpvC-Mdha and SpvC-Dha hereafter) were also constructed by simply replacing the substrate with the elimination product. The force field parameters for unnatural amino acids Mdha and Dha were generated by assigning the closely related atom types from CHARMM General force field [25].

MD simulations were performed using the CHARMM program (version c34b1) [26] with the all-hydrogen protein force field [27] including the dihedral cross-term corrections (CMAP) [28], the TIP3P water model [29], the phosphothreonine and phosphoserine parameters [30] and sodium parameters [31]. MD simulations applied 2 fs integration time step, SHAKE of covalent bonds involving hydrogen [32], periodic boundary condition (PBC) and particle mesh Ewald (PME) method [33]. All calculations used an atom-based truncation scheme updated heuristically with a list cutoff of 16 Å, a nonbond cutoff of 12 Å and with the Lennard-Jones (LJ) smoothing function initiated at 10 Å.

Any missing atoms were added using the built-in modules in CHARMM based on the topology file. The hydrogen atoms were added using HBUILD module in CHARMM. The complex system was overlaid with a 70 Å cubic water box, oriented with respect to the center of mass of protein complex; ions were added to obtain electrical neutrality. All four systems each contain approximately 37,000 atoms without considering the periodic boundary condition. The equilibration of solvated system was started by energy minimization and a 20 ps NVT MD simulation with heavy atoms of solute restrained using a force constant of 2 kcal/mol/Å^2. Following this, restraints were removed and the system was fully equilibrated by energy minimization, a 40 ps NVT MD simulation and a 20 ps NPT MD simulation using the Nosé–Hoover temperature coupling scheme. Finally, a production run of 10 ns MD simulation was performed in constant-NPT ensemble.

2.2. Truncated active-site model and QM methods

MD simulation results for SpvC-Erk2 complexed with K136 in the deprotonated state show a stable binding site including all the key residues (Fig. S4), which enable us to strike the balance between accuracy and efficiency by carrying out QM calculations with a truncated active-site model [19,34,35] to investigate the SpvC catalyzed reaction mechanisms. This model consists of all essential moieties of the substrate and key binding site residues involving in substrate binding and enzymatic reaction explicitly or implicitly, including methyl capped pT183, methylbenzene, methylammonium, 4-methylimidazoium, n-butylamine, ethane and p-methylphenol to represent substrate, and binding site residues F86, K104, H106, K136,

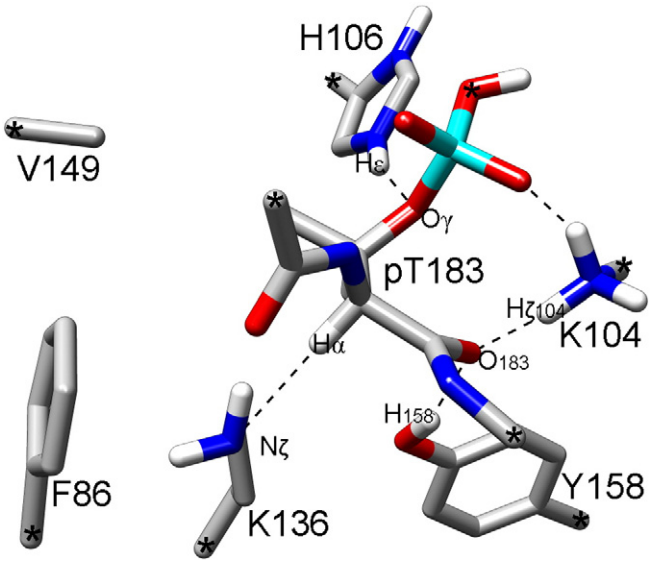

Fig. 2. Truncated active site model. The model consists methyl capped pT183, methylbenzene, methylammonium, 4-methylimidazolium, n-butylamine, ethane and p-methylphenol to represent substrate, and binding site residues F86, K104, H106, K136, V149 and Y158. The frozen terminal atoms during geometry optimization are marked with asterisk. C, O, N, H and P are colored in gray, red, blue, white and cyan, respectively. All non-polar hydrogen atoms except H_α of pT183 are omitted for clarity. Images generated with Chimera [44].

V149 and Y158, respectively (Fig. 2). The arginine residues interacting with phosphate moiety (i.e. R148, R213 and R220) were mimicked implicitly by neutralizing and fixing the position of the O_θ atom of the phosphate group, which results in the net change of binding site residues. The terminal carbon atoms of each truncated sidechain and methyl groups capped on pT183 were frozen throughout the QM geometry optimization, because the QM system is in gas phase and therefore the necessary interactions with water molecules required to hold the position of residues are not present. The initial coordinates of active-site model were based on MD simulation snapshot, containing 106 atoms in SpvC-Erk2 system (103 atoms in SpvC-T183S, correspondingly) with total charge of 1.

The SpvC catalyzed primary β-elimination reaction is the removal of the H_α from pT183, the cleavage of the C_β—O_γ bond, and results in a C_α C_β double bond containing product. The reaction mechanism was investigated by the reaction coordinates $r_{H\alpha—N\zeta}$ and $r_{H\varepsilon—O\gamma}$ (Fig. 2), defined as the distance between the proton H_α of pT183 and the basic atom N_ζ of K136, and the distance between the acidic proton H_ε from H106 and the acceptor atom O_γ from pT183, individually. The employed reaction coordinates represent the abstract of proton H_α by the putative catalytic base K136, and the donation of the proton H_ε by the putative catalytic acid H106. This designation of reaction coordinates does not specifically assign the reaction coordinate for the cleavage of H_α—C_α bond or C_β—O_γ bond.

To study the secondary reaction, the product complex of the primary elimination reaction was used. K136 was manually deprotonated and the active-site model was minimized, which leads to the reactant complex for secondary reaction. The reaction coordinate $r_{N\zeta—C\beta}$ was defined as the distance between N_ζ atom of K136 and C_β of Mdha, represents the formation of covalently bonded complex through a Michael-addition reaction mechanism [34].

The reaction energy surface was determined by adiabatic mapping, where the reaction coordinate was varied by 0.1 Å increments. All of the other geometrical variables were optimized during energy surface scanning except the reaction coordinates and the positional constraints mentioned above. Geometrical optimization was done using density functional theory (DFT/B3LYP/6-31G(d)) method [36–38]. Energy refinement was then carried out on identified key intermediate structures using MP2/6-31G(d) [39], and all the energy values reported in this manuscript were calculated using MP2 method. All QM calculations were carried out using Gaussian 03 program [40].

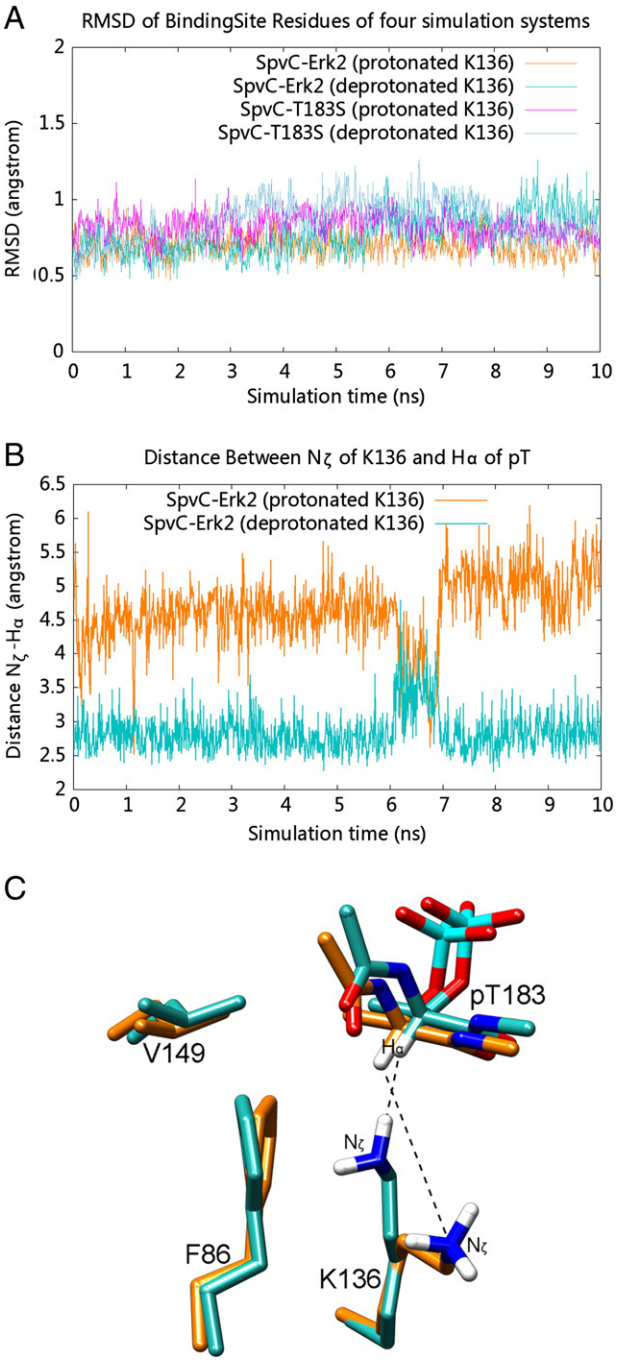

Fig. 3. A: RMSD of binding site residues and substrate in SpvC-Erk2 and SpvC-T183S with K136 in both protonated and deprotonated states. Binding site residues include F86, K104, H106, K136, R148, V149, Y158, R213, R220 and pT183. B: Distance between N_ζ of K136 and H_α of pT183 in SpvC-Erk2 with K136 in protonated (orange line) and deprotonated (turquoise line) states. C: Superimposed structures of SpvC-Erk2 with K136 in both protonated and deprotonated states. Carbon atoms are colored in orange in protonated K136 system and colored in turquoise in deprotonated K136; O, N, H and P atoms are colored in red, blue, white and cyan, respectively. Images generated with Chimera[44].

3. Results and discussion

3.1. Deprotonation of K136 coupled with the binding site reorganization

One of the outstanding questions for understanding the action of SpvC is how the positively charged lysine K136 is deprotonated in order to act as a catalytic base. We performed 10 ns MD simulations of SpvC-peptide complexes with K136 in both deprotonated and protonated states, and undertook extensive structural and energetic analyses with emphasis on the atomic events. Note that the analysis is only presented for SpvC-Erk2 if similar behaviors are observed for the T183S mutant.

Examination of the Root mean square deviation (RMSD) of the binding site residues and substrate peptides with respect to the crystal structure indicates that SpvC-peptide complex structures are stable in all four simulations (Fig. 3A); however, critical structural perturbations are observed. The most notable event occurring in the deprotonated K136 system is that the deprotonated K136 is greatly stabilized inside the fully desolvated binding pocket surrounded by conserved hydrophobic residues F86 and V149 as well as the substrate peptide, forming a stable hydrogen bond with substrate peptide (carbonyl O of A182 adjacent to pT183) and rarely interacts with solvent waters (Fig. S2). This observation is supported by a recent paper that describes a lysine that is favorable as neutral state when it is buried in a less polar microenvironment inside the protein [41]. As shown in Fig. 3B, these interactions help to stabilize the lone pair of electrons of K136 poising toward the H_α of pT183 ($r_{H\alpha—N\zeta} = 2.8 \pm 0.3$ Å). In contrast, the charged ammonium group of K136 is exposed to the solvent, forming averagely two hydrogen bonds with water molecules and rarely interacting with substrate or other binding site residues with significantly longer $r_{H\alpha—N\zeta}$ distance (4.6 ± 0.5 Å) (Fig. 3C). F86D and V149D mutants were shown to significantly decrease their enzymatic activity [11], it seems that these two hydrophobic residues not only contribute to substrate recognition, but are also involved in catalysis by stabilizing K136 in its deprotonated form. The present results suggest the deprotonation of K136 is coupled with the reorganization of the substrate binding pocket, and the deprotonated K136 is stabilized in the fully desolvated binding pocket, poises at the ideal position to abstract the alpha hydrogen atom of pT183. A similar scenario was observed for a catalytic lysine in acetoacetate decarboxylase [42].

Previous biochemical studies have demonstrated that substitution of phosphothreonine with phosphoserine compromises both peptide substrate recognition and catalytic efficiency [9]. Based on the crystallographic structures, it is evident that important interactions occur between binding site residue V149 and methyl group of pT183, which supports the binding preference of phosphothreonine over phosphoserine in this enzyme family [9,11]. Consistent with experimental observations, our MD simulations on SpvC-Erk2 and its mutant T183S reveal the atomic details in depth (Fig. 4A–B). In SpvC-Erk2, the presence of methyl group of pT183 facilitates longer lifetime of the existence of the strong interaction between H_ε of putative catalytic acid H106 and O_γ of pT183 (*ca.* 1.89 Å) comparing to SpvC-T183S (ca. 2.40 Å). Such strengthening of interaction might enhance the donation of H_ε atom of H106 to O_γ of pT183, thus promote the β-elimination reaction. Those coupled variations suggest that the hydrophobic interaction between the methyl group of pT183 and binding site residue V149 not only contributes to substrate binding, but also actively participates in primary β-elimination reaction.

3.2. The primary β-elimination reaction mechanism

The QM results of minimal energy surface along the designated reaction coordinates in SpvC-Erk2 suggest a concerted E2-like mechanism (Fig. 5A). The optimized structures of the active-site models in the reactant complex (RC), transition state (TS) and product complex (PC) states are included in Fig. 5B, and the key geometric parameters and

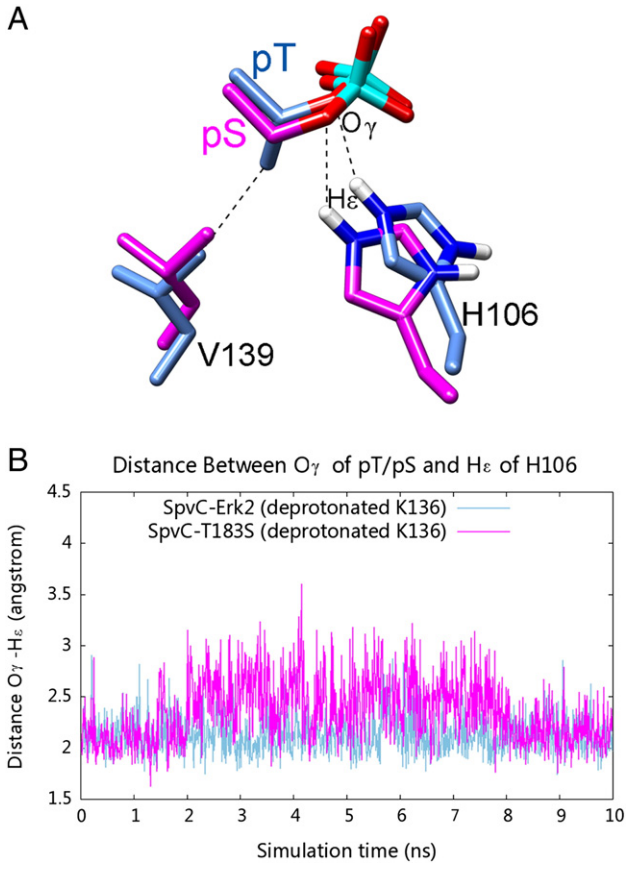

Fig. 4. A: Superimposed structures of SpvC-Erk2 and its mutant SpvC-T183S. Hydrophobic interaction between V149 and methyl group of pT stabilizes the O_γ atom poising toward the catalytic acid H106. Carbon atoms are colored in blue in SpvC-Erk2 and colored in magenta in SpvC-T183S; O, N, H and P atoms are colored in red, blue white and cyan, respectively. Images generated with Chimera [44]. B: Distance between O_γ and H_ε of H106 in simulations of SpvC-Erk2 (blue line) and SpvC-T183S (magenta line) with K136 in the deprotonated state.

energies of these stationary structures are listed in Table 1. The overall reaction mechanisms are essentially the same in SpvC-Erk2 and its T183S mutant (Fig. 5C–D). The calculated activation energy is 2 kcal/mol less in SpvC-Erk2 than in the SpvC-T183S mutant (18.22 and 20.36 kcal/mol, respectively), therefore, the eliminate reaction becomes considerably more difficult in phosphoserine containing substrate peptide, which agrees qualitatively with previous experimental observation [9]. In wild type SpvC-Erk2, the calculated activation energy is 18.22 kcal/mol, which is also close to the suggestion by experimental k_{cat} values measured in this enzyme family (~16–18 kcal/mol) [9]. Thus, the detailed analysis is only presented for SpvC-Erk2 unless otherwise noted in this subsection.

Because all hydrogen atoms were added in silico and K136 is mutated in the crystal structure of SpvC complexed with Erk2 peptide, we could not compare the distances related to the hydrogen atoms and K136 in the optimized structure of our truncated model to the crystal structure. However, the optimized structure of the reactant complex (Fig. 5B) has essentially identical geometry to its initial structure truncated from the MD snapshot. Catalytic base K136 is oriented toward H_α of pT183 ($r_{N\zeta—H\alpha} = 2.33$ Å), and catalytic acid H106 interacts favorably with pT183 ($r_{O\gamma—H\varepsilon} = 2.11$ Å). The elimination reaction is initiated from the abstraction of the H_α by K136, however, the loss of H_α and the removal of the phosphate group from pT183 do not occur until the reaction reaches the TS, where the H_α is largely transferred to K136 ($r_{N\zeta—H\alpha} = 1.13$ Å) with a nearly broken $H_\alpha—C_\alpha$ bond ($r_{C\alpha—H\alpha} = 1.79$ Å), and the $C_\beta—O_\gamma$ bond starts to cleave ($r_{C\beta—O\gamma} = 1.59$ Å) coupled with a partially forming C_α C_β double bond

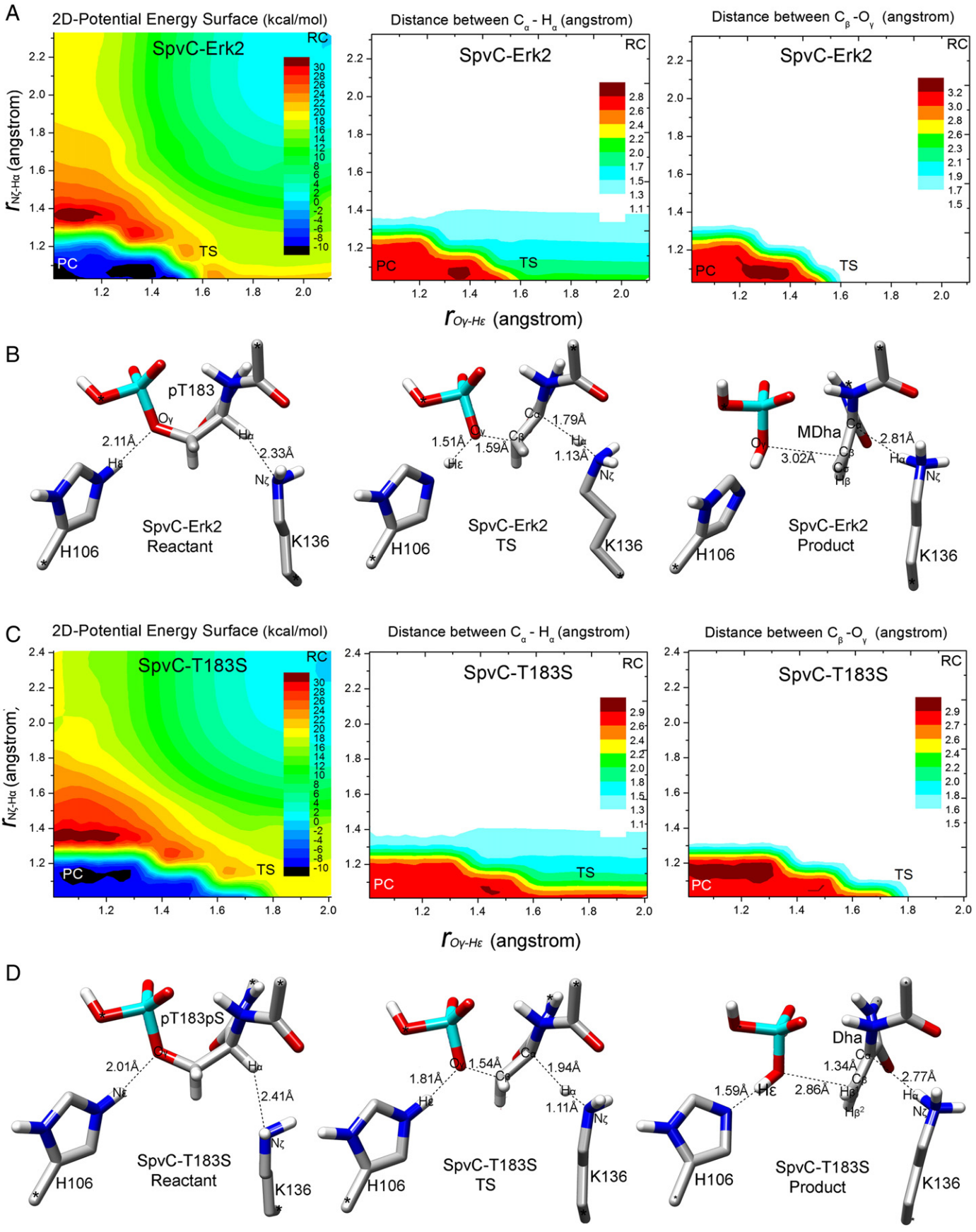
A
2D-Potential Energy Surface (kcal/mol)
SpvC-Erk2
RC
PC
TS
$r_{Nζ-Hα}$ (angstrom)
Distance between $C_α$ - $H_α$ (angstrom)
Distance between $C_β$ -$O_γ$ (angstrom)
$r_{Oγ-Hε}$ (angstrom)
B
pT183
2.11Å
2.33Å
SpvC-Erk2
Reactant
H106
K136
1.51Å
1.59Å
1.79Å
1.13Å
SpvC-Erk2
TS
MDha
3.02Å
2.81Å
SpvC-Erk2
Product
C
SpvC-T183S
D
pT183pS
2.01Å
2.41Å
SpvC-T183S
Reactant
1.81Å
1.54Å
1.94Å
1.11Å
SpvC-T183S
TS
Dha
1.59Å
2.86Å
1.34Å
2.77Å
SpvC-T183S
Product

Table 1
Key geometrical parameters and relative energies at RC, TS and PC states in the primary β-elimination reaction, individually. The improper dihedral angle ϕ_1 is defined as C_σ—H_β—C_α—C_β in SpvC-Erk2 and $H_{\beta1}$—$H_{\beta2}$—C_α—C_β in SpvC-T183S.

Systems		Distance (Å)							Improper dihedral (°)	Energy (kcal/mol)
		$r_{N\zeta—H\alpha}$	$r_{O\gamma—H\varepsilon}$	$r_{C\beta—O\gamma}$	$r_{C\alpha—C\beta}$	$r_{C\alpha—H\alpha}$	$r_{N\varepsilon—H\varepsilon}$	$r_{O183—H\zeta104}$	ϕ_1	MP2/6-31G(d)
SpvC-Erk2	RC	2.33	2.11	1.46	1.55	1.10	1.03	1.95	−36.82	0
(K104 included)	TS	1.13	1.51	1.59	1.50	1.79	1.12	1.97	−32.43	18.22
	PC	1.04	1.03	3.02	1.34	2.81	1.59	3.99	0.33	−11.19
SpvC-Erk2	RC	2.46	1.79	1.48	1.56	1.10	1.05		−36.42	0
(K104 excluded)	TS	1.37	0.99	1.60	1.51	1.36	1.83		−31.41	24.85
	PC	1.07	0.99	2.54	1.34	2.79	1.78		0.67	−3.58
SpvC-T183S	RC	2.41	2.01	1.46	1.54	1.10	1.03	1.93	−35.22	0
(K104 included)	TS	1.11	1.81	1.54	1.48	1.94	1.05	1.87	−31.98	20.36
	PC	1.06	1.02	2.86	1.34	2.77	1.59	4.37	3.42	−11.66
SpvC-T183S	RC	2.38	1.78	1.46	1.55	1.10	1.05		−34.77	0
(K104 excluded)	TS	1.29	1.08	1.56	1.49	1.48	1.66		−30.61	30.42
	PC	1.08	0.99	2.59	1.34	2.91	1.77		3.83	2.03

($r_{C\alpha\ C\beta}$ = 1.50 Å). H106 seems to stabilize the TS by strengthening the interaction with the phosphate group ($r_{O\gamma—H\varepsilon}$ = 1.51 Å), yet without losing the H_ε proton ($r_{N\varepsilon—H\varepsilon}$ = 1.12 Å). Once the transition state is crossed, the proton donation from catalytic acid H106 to phosphate group ($r_{O\gamma—H\varepsilon}$ = 1.03 Å) greatly promotes the cleavage of C_β—O_γ bond ($r_{C\beta—O\gamma}$ = 3.02 Å) and the complete loss of alpha hydrogen ($r_{C\alpha—H\alpha}$ = 2.81 Å), results in the double bond containing product ($r_{C\alpha\ C\beta}$ = 1.34 Å). The formation of the C_α C_β double bond is also indicated by the planar improper dihedral angle centered with C_β ($\phi_{C\delta—H\beta—C\alpha—C\beta}$ = 0.33°), and forms a conjugated system with the backbone carbonyl of pT183.

Binding site residues K104A mutant significantly decreases the phosphothreonine lyase activity of SpvC [9]. A recent QM study [43] proposed a SpvC catalyzed elimination mechanism with the calculated activation energy of 24.34 kcal/mol, however, their active-site model didn't include K104, and might lead to inaccurate TS determination. In our calculation, K104 forms a strong hydrogen bond with the backbone carbonyl O of pT183 (O_{183}) in both reactant and TS structures (Table 1), involves in stabilizing the TS and facilitates the reaction to occur. To assess the role of K104, we scanned the 2D QM surfaces with the K104 excluded in truncated active-site model. The key geometrical parameters and energies are included in Table 1, and minimal energy surfaces are presented in Fig. S3. Without the presence of K104, the activation energy rises to 24.85 kcal/mol in SpvC-Erk2 system, and the TS structure presents striking contrast. The reaction is initiated from the donation of proton H_ε from H106 to phosphate ($r_{H\varepsilon—O\gamma}$ = 0.99 Å), and results in the nearly broken C_β—O_γ bond ($r_{C\beta—O\gamma}$ = 1.60 Å) in TS state. Clearly, K104 plays a crucial role in determining the structural and energetic properties of TS state in SpvC catalyzed elimination reaction process.

3.3. The nucleophilic addition mechanism

In addition to the primary β-elimination product, we also detected a covalently bound complex (Fig. S1). Based on examining the structures of simulated SpvC-Erk2 complexes (Fig. 2), it is evident that the well aligned alpha hydrogen atom of pT183 blocks the path of K136 to directly attack C_β atom via a substitution reaction mechanism. Instead, K136 has potential to act as nucleophile to attack the unsaturated C_β atom of primary elimination product (PC structure at Fig. 5). Similarly, we performed MD simulations on SpvC-product complexes with K136 in both protonated and deprotonated states. The similar behaviors were observed as in SpvC-Erk2 reactant complexes, where the deprotonated K136 is stabilized inside the desolvated active site and positioned toward the C_β atom (Fig. S4).

To investigate this nucleophilic addition reaction, the reaction coordinate was designed as the distance between the nucleophile K136 and unsaturated C_β atom of elimination product ($r_{N\zeta—C\beta}$). The energy profiles and the reactant, TS and product state structures are presented in Fig. 6, the key geometric parameters and energies of these stationary structures are listed in Table 2. The presence of the methyl group in Mdha introduces unfavorable steric hindrance for K136 to attack the C_β atom, as evidence in both reactant structures and the calculated activation energies. The catalytic residue K136 is located 5.12 Å away from the C_β atom in SpvC-Mdha comparing with 3.67 Å in SpvC-Dha (Fig. 6), and the calculated activation energy is 3.6 kcal/mol higher in SpvC-Mdha than in SpvC-Dha (16.6 and 12.92 kcal/mol, respectively). Clearly, the nucleophilic addition reaction is considerably more difficult to occur in SpvC-Mdha system, which is in good agreement with our experimental results and the previous observation [9].

As the nucleophilic addition reaction mechanism is essentially the same in SpvC-Dha and SpvC-Mdha systems, the detailed analysis is only presented for SpvC-Dha. The addition reaction is initiated from the nucleophilic attack of the unsaturated C_β of Dha by catalytic residue K136. In TS structure, the newly forming single bond N_ζ—C_β ($r_{N\zeta—C\beta}$ = 1.90 Å) is coupled with the increasing bond length of C_α C_β double bond ($r_{C\alpha\ C\beta}$ = 1.40 Å) and the increasing improper dihedral angle ($\phi_{H\beta1—H\beta2—C\alpha—C\beta}$ = 21.42°), which indicates that the hybridization of C_β is changing from sp2 to sp3. A delocalized π system is forming between bond C_α—C ($r_{C\alpha—C}$ = 1.44 Å) and the neighboring carbonyl group. In our present calculation, only a product-like structure was produced as we didn't explore the rearrangement of proton $H_{\zeta1}$ further. It is likely to involve a keto-enol tautomerization due to the formed hydrogen bond between N_ζ of K136 and carbonyl O of pS183. Although the biological consequence of this suicidal reaction

Fig. 5. A: 2D energy landscape (left), $r_{C\alpha—H\alpha}$ (middle) and $r_{O\gamma—C\beta}$ (right) of the primary β-elimination reaction as a function of reaction coordinates ($r_{N\zeta—H\alpha}$ and $r_{O\gamma—H\varepsilon}$) in SpvC-Erk2. B: Optimized structures of truncated SpvC-Erk2 model at RC, TS and PC states along the β-elimination reaction pathway. K104 was omitted in the figure for clarity; it plays the role of stabilizing the TS to facilitate the reaction to occur. The distance can be found in Table 1. C: 2D energy landscape (left), $r_{C\alpha—H\alpha}$ (middle) and $r_{O\gamma—C\beta}$ (right) as a function of reaction coordinates ($r_{N\zeta—H\alpha}$ and $r_{O\gamma—H\varepsilon}$) in SpvC-T183S. D: Optimized structures of truncated SpvC-T183S model at RC, TS and PC states. K104 was omitted in the figure for clarity, it plays the role of stabilizing the TS to facilitate the reaction to occur. The distance can be found in Table 1. C, O, N, H and P are colored in gray, red, blue, white and cyan, respectively. Images generated with Chimera [44].

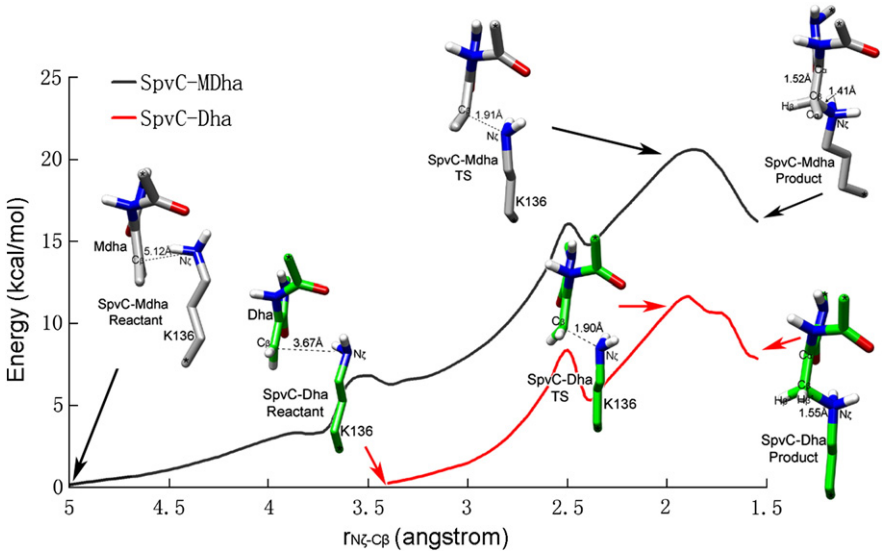

Fig. 6. Energy profiles of the secondary addition reaction with respect to the reaction coordinate $r_{N\zeta-C\beta}$ in SpvC-Mdha and SpvC-Dha complexes. Optimized structures of truncated model in RC, TS and PC states are presented for both systems. C atoms are colored in gray in SpvC-Mdha and colored in green in SpvC-Dha; O, N and H are colored in red, blue and white, respectively.

is not clear, such processive reaction mechanism used by phosphothreonine lyases might serve as a programmed regulation to fine tune their enzymatic activity.

4. Conclusions

In combination of theoretical calculations and experimental observations, a complete enzymatic pathway for SpvC catalyzed reactions is illustrated (Scheme 1). Our calculated results are in good agreement with the experimental measurements, reveal the critical stages of SpvC catalyzed reactions and reconcile the roles of several important binding site residues in catalytic reactions. Firstly, molecular dynamics simulation results indicated that the deprotonation of the catalytic residue K136 is facilitated by the formation of the fully desolvated active site upon substrate binding, thus the deprotonated K136 is stabilized and precisely located to act as a catalytic base. The hydrophobic binding site residues F86 and V149 are not only involved in substrate recognition, but also play important roles in stabilizing the deprotonated K136. Secondly, truncated active-site model was applied to explore the elimination reaction pathway using quantum mechanics method. The 2-D minimal potential energy surface, resulted from thoroughly scanning the reaction coordinates of alpha hydrogen abstraction by catalytic base K136 and proton donation by catalytic acid H106, suggests that the β-elimination occurs via an E2-like mechanism. The activation energies for the wild type substrate and its T183S mutant were estimated to be 18.22 and 20.36 kcal/mol, respectively. In this β-elimination reaction, binding site residue K104 was identified to play critical role in determining the structural and energetics of transition state. Finally, the subsequent deprotonation of K136 happens to be a natural sequel of the primary elimination reaction, restores its nucleophile capacity to attack the unsaturated C_β atom of elimination product, and leads to a covalently bound complex via a Michael-addition mechanism. The activation energies in this step for corresponding wild type substrate and its T183S mutant were calculated to be 16.0 and 12.92 kcal/mol, respectively. In contrast to its favorable role in β-elimination reaction, the methyl group in wild type substrate introduces steric hindrance for nucleophilic addition reaction to occur. Since such SpvC catalyzed enzymatic reactions are novel, our present studies may provide additional structural and mechanistic information to facilitate the development of novel antibiotics in inhibiting the pathogenic bacteria.

Supplementary materials related to this article can be found online at doi:10.1016/j.bpc.2011.04.002.

Acknowledgment

Molecular graphics images were produced using the UCSF Chimera package from the Resource for Biocomputing, Visualization, and Informatics at the University of California, San Francisco (supported by NIH P41 RR-01081). We thank Dr. Lifeng Zhao at NIBS for the helpful discussion, and the reviewers for thoughtful comments. This work was supported by the Chinese Ministry of Science and Technology "863" Grant 2008AA022313 (to N.H.), and the Supercomputing Center of CAS for computational support. The funders had

Table 2
Reaction coordinates, bond distances, dihedral angles and relative energies at RC, TS and PC states, along the secondary Michael-addition reaction pathway. ϕ_2 is the improper dihedral angle centered with C_β determined for C_σ—H_β—C_α—C_β in system SpvC-Mdha and $H_{\beta1}$—$H_{\beta2}$—C_α—C_β in system SpvC-Dha; ϕ_3 is the dihedral angle determined for C_β—C_α—C—O in both SpvC-Mdha and SpvC-Dha.

Systems		Distance (Å)				Improper dihedral (°)	Dihedral (°)	Energy (kcal/mol)
		$r_{N\zeta-C\beta}$	$r_{C\alpha-C\beta}$	$r_{C\alpha-C}$	$r_{H\zeta-O}$	ϕ_2	ϕ_3	MP2/6-31G(d)
SpvC-Mdha	RC	5.12	1.34	1.50	2.15	2.01	21.22	0
	TS	1.91	1.40	1.43	2.64	20.64	−0.79	16.60
	PC	1.41	1.52	1.38	1.58	30.02	−13.68	4.39
SpvC-Dha	RC	3.67	1.34	1.50	2.68	0.09	−6.58	0
	TS	1.90	1.40	1.44	3.01	21.42	3.61	12.92
	PC	1.55	1.47	1.39	1.86	35.91	2.11	1.02

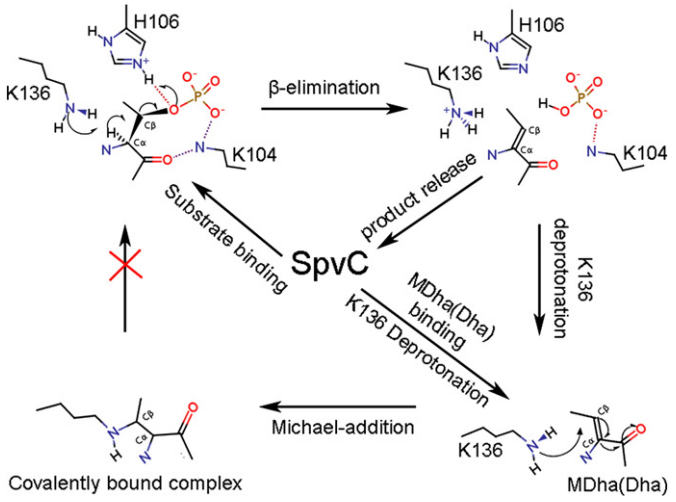

Scheme 1. Schematic diagram of the complete SpvC catalyzed reactions; the primary reaction is a β-elimination reaction via E2 mechanism; the secondary reaction is a Michael-addition initialized from the product of the primary reaction and suicidally breaks the enzymatic cycle. Both reactions use deprotonated K136 as catalytic residue, however, K136 acts as catalytic base in primary elimination reaction while a nucleophile in secondary addition reaction.

no role in study design, data collection and analysis, decision to publish, or preparation of the manuscript.

References

[1] A. Shizuo, U. Satoshi, T. Osamu, Pathogen recognition and innate immunity, Cell 124 (2006) 783.
[2] J.D. Ashwell, The many paths to p38 mitogen-activated protein kinase activation in the immune system, Nat. Rev. Immunol. 6 (2006) 532.
[3] F.M. Ausubel, Are innate immune signaling pathways in plants and animals conserved? Nat. Immunol. 6 (2005) 973.
[4] G. Tena, T. Asai, W.-L. Chiu, J. Sheen, Plant mitogen-activated protein kinase signaling cascades, Curr. Opin. Plant Biol. 4 (2001) 392.
[5] C. Dong, R.J. Davis, R.A. Flavell, Map Kinase in the immune response, Annu. Rev. Immunol. 20 (2002) 55.
[6] L. Shan, P. He, J. Sheen, Intercepting host MAPK signaling cascades by bacterial type III effectors, Cell Host Microbe 1 (2007) 167.
[7] L. Arbibe, D.W. Kim, E. Batsche, T. Pedron, B. Mateescu, C. Muchardt, C. Parsot, P.J. Sansonetti, An injected bacterial effector targets chromatin access for transcription factor NF-kappaB to alter transcription of host genes involved in immune responses, Nat. Immunol. 8 (2007) 47.
[8] R.W. Kramer, N.L. Slagowski, N.A. Eze, K.S. Giddings, M.F. Morrison, K.A. Siggers, M.N. Starnbach, C.F. Lesser, Yeast functional genomic screens lead to identification of a role for a bacterial effector in innate immunity regulation, PLoS Pathog. 3 (2007) e21.
[9] Y. Zhu, H. Li, C. Long, L. Hu, H. Xu, L. Liu, S. Chen, D.-C. Wang, F. Shao, Structural insights into the enzymatic mechanism of the pathogenic MAPK phosphothreonine lyase, Mol. Cell 28 (2007) 899.
[10] J. Zhang, F. Shao, Y. Li, H. Cui, L. Chen, H. Li, Y. Zou, C. Long, L. Lan, J. Chai, S. Chen, X. Tang, J.-M. Zhou, A *Pseudomonas syringae* effector inactivates MAPKs to suppress PAMP-induced immunity in plants, Cell Host Microbe 1 (2007) 175.
[11] L. Chen, H. Wang, J. Zhang, L. Gu, N. Huang, J.-M. Zhou, J. Chai, Structural basis for the catalytic mechanism of phosphothreonine lyase, Nat. Struct. Mol. Biol. 15 (2008) 101.
[12] H. Li, H. Xu, Y. Zhou, J. Zhang, C. Long, S. Li, S. Chen, J.-M. Zhou, F. Shao, The phosphothreonine lyase activity of a bacterial type III effector family, Science 315 (2007) 1000.
[13] A.L. Osterman, H.B. Brooks, L. Jackson, J.J. Abbott, M.A. Phillips, Lysine-69 plays a key role in catalysis by ornithine decarboxylase through acceleration of the Schiff base formation, decarboxylation, and product release steps, Biochemistry 38 (1999) 11814.
[14] S. Kolappan, J. Zwahlen, R. Zhou, J.J. Truglio, P.J. Tonge, C. Kisker, Lysine 190 is the catalytic base in MenF, the menaquinone-specific isochorismate synthase from *Escherichia coli*: implications for an enzyme family, Biochemistry 46 (2007) 946.
[15] M.T. Black, Evidence that the catalytic activity of prokaryote leader peptidase depends upon the operation of a serine-lysine catalytic dyad, J. Bacteriol. 175 (1993) 4957.
[16] D. Alexeev, R. Baxter, D. Campopiano, O. Kerbarh, L. Sawyer, N. Tomczyk, R. Watt, S. Webster, Suicide inhibition of alpha-oxamine synthases: structures of the covalent adducts of 8-amino-7-oxononanoate synthase with trifluoroalanine, Org. Biomol. Chem. 4 (2006) 1209.
[17] K.-H. Tang, S.O. Mansoorabadi, G.H. Reed, P.A. Frey, Radical triplets and suicide inhibition in reactions of 4-Thia-d- and 4-Thia-l-lysine with lysine 5,6-aminomutase, Biochemistry 48 (2009) 8151.
[18] J.L. Klepeis, K. Lindorff-Larsen, R.O. Dror, D.E. Shaw, Long-timescale molecular dynamics simulations of protein structure and function, Curr. Opin. Struct. Biol. 19 (2009) 120.
[19] D. Xu, H. Guo, Q. Cui, 1. Antibiotic deactivation by a dizinc β-lactamase: mechanistic insights from QM/MM and DFT studies, J. Am. Chem. Soc. 129 (2007) 10814.
[20] R.A. Friesner, V. Guallar, Ab initio quantum chemical and mixed quantum mechanics/molecular mechanics (QM/MM) methods for studying enzymatic catalysis, Annu. Rev. Phys. Chem. 56 (2005) 389.
[21] J. Gao, S. Ma, D.T. Major, K. Nam, J. Pu, D.G. Truhlar, Mechanisms and free energies of enzymatic reactions, Chem. Rev. 106 (2006) 3188.
[22] Y. Yang, Q. Cui, The hydrolysis activity of adenosine triphosphate in myosin: a theoretical analysis of anomeric effects and the nature of the transition state, J. Phys. Chem. A 113 (2009) 12439.
[23] O. Acevedo, W.L. Jorgensen, Advances in quantum and molecular mechanical (QM/MM) simulations for organic and enzymatic reactions, Acc. Chem. Res. 43 (2010) 142.
[24] G. Roos, P. Geerlings, J. Messens, Enzymatic catalysis: the emerging role of conceptual density functional theory, J. Phys. Chem. B 113 (2009) 13465.
[25] K. Vanommeslaeghe, E. Hatcher, C. Acharya, S. Kundu, S. Zhong, J. Shim, E. Darian, O. Guvench, P. Lopes, I. Vorobyov, A.D. Mackerell Jr., CHARMM general force field: a force field for drug-like molecules compatible with the CHARMM all-atom additive biological force fields, J. Comput. Chem. 31 (2009) 671.
[26] B.R. Brooks, R.E. Bruccoleri, B.D. Olafson, D.J. States, S. Swaminathan, M. Karplus, CHARMM: a program for macromolecular energy, minimization, and dynamics calculations, J. Comput. Chem. 4 (1983) 187.
[27] A.D. MacKerell Jr., B. Brooks, C.L. Brooks III, L. Nilsson, B. Roux, Y. Won, M. Karplus, CHARMM: the energy function and its parameterization with an overview of the program, The encyclopedia of Computational Chemistry, 1, Wiley, New York, 1998.
[28] A.D. MacKerell Jr., M. Feig, C.L. Brooks III, Extending the treatment of backbone energetics in protein force fields: Limitations of gas-phase quantum mechanics in reproducing protein conformational distributions in molecular dynamics simulations, J. Comput. Chem. 25 (2004) 1400.
[29] W.L. Jorgensen, J. Chandrasekhar, J.D. Madura, R.W. Impey, M.L. Klein, Comparison of simple potential functions for simulating liquid water, J. Chem. Phys. 79 (1983) 926.
[30] M.-H. Feng, M. Philippopoulos, A.D. MacKerell, C. Lim, Structural characterization of the phosphotyrosine binding region of a high-affinity SH2 domain-phosphopeptide complex by molecular dynamics simulation and chemical shift calculations, J. Am. Chem. Soc. 118 (1996) 11265.
[31] D. Beglov, B. Roux, An integral equation to describe the solvation of polar molecules in liquid water, J. Phys. Chem. B 101 (1997) 7821.
[32] J.-P. Ryckaert, G. Ciccotti, H.J.C. Berendsen, Numerical integration of the Cartesian equations of motion of a system with constraints: molecular dynamics of n-alkanes, J. Comput. Phys. 23 (1977) 327.
[33] U. Essmann, L. Perera, M. Berkowitz, T. Darden, H. Lee, L. Pedersen, A smooth particle mesh Ewald method, J. Chem. Phys. 103 (1995) 8577.
[34] A.G. Taranto, P. Carvalho, M.A. Avery, QM/QM studies for Michael reaction in corona virus main protease (3CLPro), J. Mol. Graph. Mod. 27 (2008) 275.
[35] H. Guo, Q. Cui, Antibiotic binding to dizinc β-lactamase L1 from *Stenotrophomonas maltophilia*: SCC-DFTB/CHARMM and DFT studies, J. Phys. Chem. A 111 (2007) 5630.
[36] A.D. Becke, Density-functional exchange-energy approximation with correct asymptotic behavior, Phys. Rev. A 38 (1988) 3098.
[37] A.D. Becke, Density-functional thermochemistry. V. Systematic optimization of exchange-correlation functionals, J. Chem. Phys. 107 (1997) 8554.
[38] C. Lee, W. Yang, R.G. Parr, Development of the Colle–Salvetti correlation-energy formula into a functional of the electron density, Phys. Rev. B 37 (1988) 785.
[39] C. Møller, M.S. Plesset, Note on an approximation treatment for many-electron systems, Phys. Rev. 46 (1934) 618.
[40] M.J. Frisch, G.W. Trucks, H.B. Schlegel, G.E. Scuseria, M.A. Robb, J.R. Cheeseman, J.J.A. Montgomery, K.N.K.T. Vreven, J.C. Burant, J.M. Millam, S.S. Iyengar, J. Tomasi, V. Barone, B. Mennucci, M. Cossi, G. Scalmani, N. Rega, G.A. Petersson, H. Nakatsuji, M. Hada, M. Ehara, K. Toyota, R. Fukuda, J. Hasegawa, M. Ishida, T. Nakajima, Y. Honda, O. Kitao, H. Nakai, M. Klene, X. Li, J.E. Knox, H.P. Hratchian, J.B. Cross, V. Bakken, C. Adamo, J. Jaramillo, R. Gomperts, R.E. Stratmann, O. Yazyev, A.J. Austin, R. Cammi, C. Pomelli, J.W. Ochterski, P.Y. Ayala, K. Morokuma, G.A. Voth, P. Salvador, J.J. Dannenberg, V.G. Zakrzewski, S. Dapprich, A.D. Daniels, M.C. Strain, O. Farkas, D.K. Malick, A.D. Rabuck, K. Raghavachari, J.B. Foresman, J.V. Ortiz, Q. Cui, A.G. Baboul, S. Clifford, J. Cioslowski, B.B. Stefanov, G. Liu, A. Liashenko, P. Piskorz, I. Komaromi, R.L. Martin, D.J. Fox, T. Keith, M.A. Al-Laham, C.Y. Peng, A. Nanayakkara, M. Challacombe, P.M.W. Gill, B. Johnson, W. Chen, M.W. Wong, C. Gonzalez, J.A. Pople, Gaussian 03, Revision C.02, Gaussian, Inc, Wallingford CT, 2004.
[41] D.G. Isom, C.A. Castañeda, B.R. Cannon, B. García-Moreno, Large shifts in pKa values of lysine residues buried inside a protein, Proc. Natl. Acad. Sci. 108 (2011) 5260.
[42] M.-C. Ho, J.-F. Menetret, H. Tsuruta, K.N. Allen, The origin of the electrostatic perturbation in acetoacetate decarboxylase, Nature 459 (2009) 393.
[43] G.K. Smith, Z. Ke, A.C. Hengge, D. Xu, D. Xie, H. Guo, Active-site dynamics of SpvC virulence factor from *Salmonella typhimurium* and density functional theory study of phosphothreonine lyase catalysis, J. Phys. Chem. B 113 (2009) 15327.
[44] E.F. Pettersen, T.D. Goddard, C.C. Huang, G.S. Couch, D.M. Greenblatt, E.C. Meng, T.E. Ferrin, UCSF Chimera—a visualization system for exploratory research and analysis, J. Comput. Chem. 25 (2004) 1605.